Egypt. J. Chem. **Vol. 66**, No. 10 pp. 149 - 161 (2023)

Egyptian Journal of Chemistry

http://ejchem.journals.ekb.eg/

In Vitro and *In Silico* studies of Neophytadiene; A Diterpene Isolated from *Aeschynomene Elaphroxylon* (Guill. &Perr.) Taub. as Apoptotic

Ahmed Hany Selmy[1]*,Mostafa Mahmoud Hegazy[1],Atef Ahmed El-Hela[1],Abdulrahman M. Saleh[2],Mohamed M. El-Hamouly[1]

[1]*Department of Pharmacognosy and medicinal plants, Faculty of Pharmacy (Boys), Al-Azhar University, Cairo 11884, Egypt*

[2]*Department of Pharmaceutical Medicinal Chemistry and Drug Design, Faculty of Pharmacy (Boys), Al-Azhar University, Cairo 11884, Egypt*

Abstract

Aeschynomene elaphroxylon (Guill. & Perr.) Taub. is a large aquatic shrub native to Madagascar and tropical Africa and cultivated in Egypt. Petroleum ether extract showed remarkable cytotoxic activities against human lung carcinoma (A-549), and prostate carcinoma cells (PC-3) with IC_{50} values 12.3±0.8 and 23.8±1.2 µg/ml, respectively. So, pet. ether extract was furtherly fractionated affording seven fractions, tested for cytotoxic activity against A-549, and PC-3. The sub-fraction (PET-5) from pet. ether fraction showed potent cytotoxic activities more than cisplatin against A-549, and PC-3 with IC_{50} values 6.94±0.48 and 7.33±0.58 µg/ml, respectively. The major compound of sub-fraction PET-5 was identified by GCMS as Neophytadiene (1) at percentage of 82.23 %. *In silico* studies showed that neophytadiene blocks three receptors which have main role in cancer viability, invisibility as it blocks Human A2a receptor at adenosine binding site, Human LRH1 and hERG K+ channel leads to inhibition of cancer proliferation and invasiveness which may act as a promising apoptotic inducer. The phytochemical investigation of the plant major fractions resulted in isolation of five compounds. From pet. ether fraction (1) Neophytadiene was identified, from ethyl acetate fraction (2) Kaempferol-7-O-*α*-L-rhamnoside and (3) Medicarpin-3-O-*β*-D-glucopyranoside were isolated and from n-butanol fraction (4) kaempferol 3-O-*β*-D-apiofuranosyl-7-O-*α*-L-rhamnoside, (5) Kaempferol 3,7-di-O-*α*-L-rhamnoside were isolated.

Keywords: Neophytadiene; Diterpene; Cytotoxicity; Apoptosis; Docking; Fabaceae

1.Introduction

Cancer is considered as a major health problem especially in the developing countries. The most prevalent types of cancer are lung, colorectal and prostate(1, 2).Based on GLOBOCAN estimations in 2020 the worldwide mortality rate due to cancer was 9,958,133 deaths (3). So, the development of new anticancer drugs is a crucial demand and big challenge. Nature is an inexhaustible source of compounds that have a structural diversity with possibilities of new chemical entities discovery (4). Several marketed anticancer drugs are derived from natural sources such as paclitaxel, Vinca alkaloids and camptothecin (2).Fabaceae secondary metabolites exhibit some biological activities for the treatment of many diseases, showing antidiabetic, anti-inflammatory, anti-tumor, antiproliferative, antiviral and antimicrobial activity(5). Fabaceae is rich in various phytochemicals such as flavonoids, saponins, alkaloids and phenolic acids which showed many biological activities especially on cancer through various mechanisms such as immunomodulatory effects, inactivation of carcinogens, anti-oxidant stress, induction of apoptosis and cell cycle arrest (6, 7). Many defensive mechanisms include apoptosis as a significant part of

*Corresponding author e-mail: Drahselmy@yahoo.com.; (Ahmed Hany Selmy)
EJCHEM use only: Received date 10 December 2022; revised date 15 January 2023; accepted date 25 January 2023
DOI: 10.21608/EJCHEM.2023.178261.7296

their processes in response to many physiological and pathological stimulus such as immune reactions or cells damaging by toxic agents or diseases. So, apoptosis induction is one of the targeted strategies in the development of new drugs for treatment of cancer (8). Neophytadiene is classified as a diterpenoid compound which present in many plants and marine algae (9, 10). Neophytadiene was identified in the fractions responsible for cytotoxicity of Senna spp. (Fabaceae) which tested against human glioblastoma and human colon cancer cell lines (10). Essential oil of Rubia tinctorum was showed potent cytotoxic effect on (MOLT4v) cell line which contained neophytadiene as one of the major components that identified by GCMS (11). It was notable that the fractions of Antarctic Algae Desmarestia antarctica containing higher concentrations of neophytadiene showed stronger cytotoxic effects in Vero cells (10). Also, it was present in essential oil of Hedyotischrysotricha that gave cytotoxic effect against A-549 lung cancer cells (12). Moreover, it showed promising antiparasitic effects (10) and significant inhibition of nitric oxide production and inflammatory cytokines TNF-α, IL-6 and IL-10 both in *in vivo* and *in vitro* (13). *Aeschynomeneelaphroxylon* (Guill. & Perr.) Taub. is an aquatic large shrub up to 9 –12 m tall, it is cultivated in Egypt and South America, native to tropical Africa that belongs to Fabaceae family. It was reported that *Aeschynomene*genus plants showed hepatoprotective, cytotoxic, antimicrobial, antioxidant and anti-inflammatory activities (14). The Molecular modelling is one of the most important techniques used to simulate and imaging the expected binding mode of the compounds to the target sites in the process of developing drugs from natural compounds (15) . In molecular docking many targets could be beneficial for testing the anticancer activity such as A2a receptor Human LRH1 and hERG K+ channel (16-18). Adenosine binds to A2a receptor leading to protection of the cancer cell from T-lymphocytes attack by accumulation of intracellular cAMP that inhibits the antitumour T cells (19). A2a receptor has important role as negative feedback loop (regulator) in cancer immune response and decrease the inflammatory cytokines (INF GAMA – TNF ALPHA- IL-2 and IL-6) lead to decrease apoptosis and increase tumour growth (17). The T effector cells (Teff) inhibited by extracellular adenosine which catalysed by ectoenzymes CD39 and CD73 expressed on the T regulatory cells (Treg). Extracellular adenosine produced by cancer tissue inhibits TCR-activated antitumour T cells in the inflammatory or tumour microenvironment. Extracellular AMP adenosine production is mediated by CD39 ectoenzyme and generation of extracellular adenosine from extracellular AMP is mediated by CD73 ectoenzyme. Interferon-gamma (IFN-γ) production by antitumor T cells mediated by release of CD8+ T cells; IFN-γ enhance CD8+ T cells function and inhibits vascularization of cancer cell. So, using blocker for A2a receptor retard tumor growth and metastasis (20, 19, 21). Additionally, the human ether-a-go-go-related gene potassium channel (hERG) is a voltage dependent K+ channel. It has a critical role in tumor proliferation and cancer growth regulation; involving different signalling pathways that lead to cancer cell proliferation, survival, metastasis, secretion, and invasiveness. It was observed that hERG protein levels found to be overexpressed in cancerous cells compared to that in non-cancerous cells; this overexpression correlates with clinicopathological features in different tumors. hERG K^+ channels are considered as a novel target for cancer treatment. So, the blocking of the active site of hERG K+ channels results in a successful inhibition of cancer proliferation (16, 22-24). Moreover, nuclear receptor Liver receptor homolog-1 (LRH-1) is an essential regulator of gene transcription activates some signalling pathways that affect tumor viability and metastatic progression by regulation of some specific genes transcriptions (18). LRH-1 has main relationship with cancer cell proliferation and metastasis like breast, pancreatic and colorectal carcinomas so the activation of LRH-1 induces the expression of cell-cycle regulators that might facilitate cell proliferation and promote cancer development. LRH-1 physically binds to β-catenin and they exert their functions synergistically in the regulation of certain target genes and associated with human gastrointestinal cancer (25-27, 18). Additionally LRH1 promoted MDC1 transcription enhancing breast cancer cell chemoresistance and DNA damage attenuation (28). So, blockage of Human A2a receptor at adenosine binding site, Human LRH1 and hERG K+ channel led to induce the apoptosis and cancer cell death (25).

2. Experimental section

Plant material and extract preparation

Aeschynomene elaphroxylon (Guill. & Perr.) Taub. aerial parts were collected during March-April 2019 from Orman Botanical Garden Lake, Giza, Egypt. The plant material was kindly identified by Dr. Mohamed Gibali, consultant and botanist at Orman Botanical Garden. A voucher specimen (code, AE-319) was deposited in the herbarium of the Department of Pharmacognosy and Medicinal Plants, Faculty of Pharmacy, Al-Azhar University. *A.elaphroxylon* aerial parts air dried in shade at room temperature 25 °C for 15 days, powdered mechanically by electric grain mill (25 000 rpm, 1 min) with mesh size 2mm (model 750A California, USA).

The powdered material (1.4 kg) was weighed precisely in a digital balance (Sartorius electrical balance TE 2145, Hanover, Germany) 1.4 kg then powder macerated in 70% methanol for 10 days with occasional shaking and stirring, methanolic part was filtered and concentrated under vacuum at 40 °C tell dryness using an evaporator (Heidolph, WB 2000, Germany). The crude methanol extract with the yield of 103.6 g equals 7.14 % (w/w) was weighed accurately then stored at – 18 °C for phytochemical and biological investigations.

Cytotoxic activities using MTT assay

The cell proliferation studies of total extract, pet. ether, ethyl acetate, n-butanol and seven sub-fractions of pet. ether of *A.elaphroxylon* were tested against different cancer cell lines; MCF-7 cells (human breast carcinoma), A-549 cells (human Lung carcinoma), PC-3 cells (human Prostate carcinoma) and CHO-K1 cells (human Ovary carcinoma) were obtained from VACSERA Tissue Culture Unit where Cisplatin was used as positive control with a series of concentration (from 0 -250 µg/ml), DMEM (Dulbeco's modified eagles' medium) with 10% heat-inactivated fetal bovine serum (FBS), 1% L-glutamine, HEPES buffer and 50µg/ml gentamycin were maintained for cell lines , the cells were seeded in 96-well plate at a cell concentration of 1×104 cells per well in 100µl of growth medium and incubated at 37 ºC under a humidified atmosphere of 5% of CO2 for 24 h. Therefore, the major fractions, 7 sub-fractions of petroleum ether and positive controls were dissolved in 2.5% DMSO where DMSO was used as negative control fractions and sub-fractions with series of concentrations (from 0- 250 µg /mL) and positive control at the concentrations (from 0-250 µg /mL) were added and incubated for 24 h. In brief, after the incubation period ended, the media were aspirated and the crystal violet solution (1%) was added to each well for at least 30 minutes. The stain was removed and we rinsed the plates using tap water until all excess stain is completely removed then Glacial acetic acid (30%) was added to all wells and mixed thoroughly, and then the plates absorbance were measured after gently shaken on Microplate reader (TECAN, Inc.), using wavelength of 490 nm. All results were corrected for background absorbance detected in wells without added stain. Treated samples were compared with the cell control in the absence of the tested compounds. All experiments were done 3 times. The cell cytotoxic effect of each tested sample was calculated.

The optical density was measured with the microplate reader (SunRise, TECAN, Inc, USA) to determine the number of viable cells and the percentage of viability was calculated as [(ODt/ODc)]x100% where ODt is the mean optical density of wells treated with the tested sample and ODc is the mean optical density of untreated cells. The relation between surviving cells and drug concentration is plotted to get the survival curve of each tumor cell line after treatment with the specified samples. The 50% inhibitory concentration (IC_{50}), the concentration required to cause toxic effects in 50% of intact cells, was estimated from graphic plots of the dose response curve for each conc. using GraphPad Prism software (San Diego, CA. USA) (29, 30).

Determination of total phenolic and flavonoid contents

The concentration of total phenolic compounds in the methanolic extract was determined spectrophotometrically using the Folin-Ciocalteu reagent (Sigma Chemical Co., St. Louis, MO, USA) which used for the colorimetric assay of phenolic and polyphenols (31) using different concentrations of gallic acid (10- 50µg/ml) in methanol. Their absorbance was measured at 725 nm using 95% ethanol as blank and the results expressed in terms of gallic acid equivalent. Determination of the total flavonoid content in the methanolic extract was done by colorimetric assay with 2% aluminum chloride solution in methanol (32) using different concentrations of quercetin in methanol (100- 200 µg/ml). Absorbance was measured at 415 nm and the results were expressed in terms of quercetin equivalent.

3.Isolation and Identification

The total methanolic extract which was suspended in distilled water (500 ml) and partitioned successively with pet. ether, ethyl acetate and n-butanol and the resultant fractions were evaporated to dryness to yield 44.5g, 7g, and 18g, respectively, 1 gm of total extract was reserved for biological studies. The total methanolic extract and major fractions were tested for cytotoxic activity against four cell lines and the petroleum ether fraction was the most promising one for further investigations. Using biologically guided fractionation of petroleum ether fraction, compound 1 was identified by GCMS as the major constituent at percentage of 82.23% in sub-fraction PET-5 which showed the most potent activity against human lung carcinoma (A-549), and prostate carcinoma cells (PC-3).

GCMS analysis was carried out using Shimadzu GCMS-QP2020 (Tokyo, Japan). The GC was equipped with Rtx-1MS fused bonded column (30 m x 0.25 mm i.d. x 0.25 µm film thickness) (Restek, USA) and a split–splitless injector. The initial temperature of the column was maintained at 45 °C for 2 min (isothermal) and programmed to 300 °C at a rate of 5 °C/min and kept constant (isothermal) at 300 °C for 5 min. Injector temperature was 250 °C. The flow rate of Helium carrier gas was 1.41 ml/min. All the mass spectra were recorded applying the following condition: (equipment current) filament emission current, 60 mA; ionization voltage, 70 eV; ion source, 200°C. Diluted samples (1% v/v) were injected with split mode (split ratio 1: 15). Chromatographic fractionation of ethyl acetate extract over polyamide column yielded four fractions, three fractions were further subjected separately to a series of column chromatographic techniques including open silica column chromatography, normal SPE, reversed SPE and gel filtration (Sephadex LH-20) to afford 2 compounds (2, 3). Chromatographic fractionation of n-butanol extract over polyamide column yielded four fractions, the sub-fraction number 1 furtherly subjected to silica gel column yielding four sub-fractions which subjected separately to a series of column chromatographic techniques including open silica column chromatography, normal SPE, reversed SPE and gel filtration (Sephadex LH-20) to afford 2 compounds (4,5).

The structures of the isolated compounds were established by chemical and on the basis and spectral data interpretation including (^{1}H-NMR, 400 MHz), (^{13}C, APT-NMR, 100 MHz) and (EI-MS, ESI-MS) for isolated compounds (1-5) were established by comparing their spectral data to those given in the literatures.

4.Molecular Docking Analysis

The effective target sites of proteins were selected based on the predictions of different targets using Swiss Target prediction. With MOE 19.0901 Software, preparation and validation of proteins and neophytadiene were estimated to perform the molecular docking inside the pockets of (Human A2a Receptor- Human LRH1 LBD- hERG K+ channel) (33). In the crystal protein structure, the binding sites were created by co-crystallizing the ligand with the crystal protein (PDB codes: 2ydo- 3plz- 2n7g). Initially, water molecules have been removed from the complex. then, quick preparation option was used to correct crystallographic disorders and unfilled valence atoms. Protein energy was minimized by applying MMFF94 force fields (34). Hence, the rigid structure of protein was obtained by applying fixed atom constraint. the essential amino acids were defined and assigned for the molecular docking process. Using Chem-Bio Draw Ultra17.0, 2D structure of tested compound was drawn and saved as SDF file. Using MOE 19.0901 software, the saved files were opened, 3D structure was protonated, and 0.1 RMSD kcal/mol. energy was minimized by the MMFF94 force field. Then, the minimized structure was prepared for docking via the ligand preparation order. The docking process was carried out through the docking option. The receptors were held rigid while the ligand was allowed to be flexible. During the refinement of docked molecule was allowed to produce ten different interaction poses with the protein. Then docking scores (affinity energy) of the best-fitted poses with the active site at (Human A2a Receptor- Human LRH1 LBD- hERG K+ channel) were recorded and 3D views were generated by Discovery Studio 2019 Client software (35). We use all these processes to predict the proposed binding mode, affinity, preferred orientation of each docking pose and binding Free energy (ΔG) of the tested compound with (Human A2a Receptor- Human LRH1 LBD- hERG K+ channel).

5.Results and Discussion

MTT assay

Cytotoxic activity of *A. elaphroxylon* extracts (total methanol, pet. ether, ethyl acetate and n-butanol) were evaluated towards four carcinoma cells; human breast carcinoma (MCF-7), prostate carcinoma cells (PC-3), human lung carcinoma (A-549) and ovary carcinoma (CHO-KI) using viability assay and the results were shown in Table 1. The pet. ether extract showed potent cytotoxic activities than positive standard (cisplatin) against prostate carcinoma cells (PC-3) and human lung carcinoma (A-549) with IC_{50} values 23.8±1.2 and 12.3±0.8 µg/ml, respectively. The total methanol extract showed strong activity towards human lung carcinoma (A-549), and prostate carcinoma cells (PC-3) with IC_{50} values 19±1.4 and 28.4±1.1 µg/ml, respectively. On the other hand, ethyl acetate and n-butanol fractions showed week cytotoxic activities against all carcinoma cancer cells.

Table (1)

IC_{50} values (µg/ml) of different extracts of *A. elaphroxylon* towards different cell lines (MCF-7, PC-3, CHO-KI and A-549)

Sample Code	IC_{50} values (µg/ml)			
	MCF-7	PC-3	CHO-KI	A-549
1	30.4±2.7	28.4±1.1	60.4±2.6	19±1.4
2	26.1±2.4	23.8±1.2	24.5±1.1	12.3±0.8
3	116±3.3	89.9 ± 3.4	121±3.2	56.1±1.9
4	103±3.1	62.1±2.7	118±3.6	61.2±2.7
Cisplatin	5.9±0.7	42.4±1.8	9.65±0.74	24.6±0.8

1= Total extract 2= Pet. ether extract
3 = Ethyl acetate extract 4= n-butanol extract

The pet. ether extract showed remarkable cytotoxic activities against human lung carcinoma (A-549), and prostate carcinoma cells (PC-3) with IC_{50} values 12.3±0.8 and 23.8 ±1.2 µg/ml. So, the pet. ether extract was furtherly fractionated using column chromatography (SPE, normal phase) to afford seven fractions that tested for their cytotoxic activity against A-549 and PC-3 cell lines. Sub-fraction PET-5 showed potent cytotoxic activities more than cisplatin against A-549 and PC-3 cell lines with IC_{50} values 6.94±0.48 and 7.33±0.58 µg/ml, respectively. The major compound of sub-fraction PET-5 was identified by GCMS as Neophytadiene (1) at percentage of 82.23 %. The Relative percentages of the identified compound in the sub-fraction PET-5 was calculated based on the total peak area in the chromatogram.

Table (2)

IC_{50} values (µg/ml) of different sub-fractions of pet. ether extract of *A. elaphroxylon* towards A-549 and PC-3 cell lines

Sub-fraction No.	IC_{50} values (µg/ml) A-549	IC_{50} values (µg/ml PC-3
PET-1	44.4±3.2	48.4±3.2
PET-2	35±3.3	36±3.3
PET-3	30±2.2	28±2.2
PET-4	52.9±4.8	60.9±4.8
PET-5	6.94±0.48	7.33±0.58
PET-6	25.6±1.8	25.6±1.8
PET-7	11.9±1.7	11.9±1.7
Cisplatin	22.1+1.2	39.7+0.9

Total phenolic and flavonoid contents

The total flavonoid content (TFC) highest value was found to be 14.05 ± 0.87 µg /gm quercetin equivalent (QE) for ethyl acetate extract and the lowest TFC value was found to be 10.43 ± 0.51 µg /gm QE for pet. ether. the highest value of total phenolic content (TPC) was 23.36 ± 1.42 mg/gm gallic acid equivalent (GAE) for total extract and the lowest value was 16.29 ± 1.37 mg/gm GAE for pet. Ether.

Table (3)

Total flavonoid and total phenolic content

Sample	Total Flavonoids Contents (µg /gm) QE	Total PhenolicContents (mg/gm) GAE
1- Pet. Ether	10.43 ± 0.51	16.29 ± 1.37
2- Ethyl acetate extract.	14.05 ± 0.87	20.42 ± 1.64
3- n–butanol extract	12.64 ± 0.92	19.47 ± 1.31
4- Total extract	13.45 ± 0.91	23.36 ± 1.42

The reported values are mean ± S.D. of three different readings

Spectral data of isolated compounds

Five compounds were identified as: (1) Neophytadiene, (2) Kaempferol-7-O-α-L-rhamnoside, (3) Medicarpin-3-O-β-D-glucopyranoside, (4) kaempferol-3-O-β-D-apiofuranosyl-7-O-α-L-rhamnoside, (5) Kaempferol-3,7-di-O-α-L-rhamnoside
(Fig. 1).

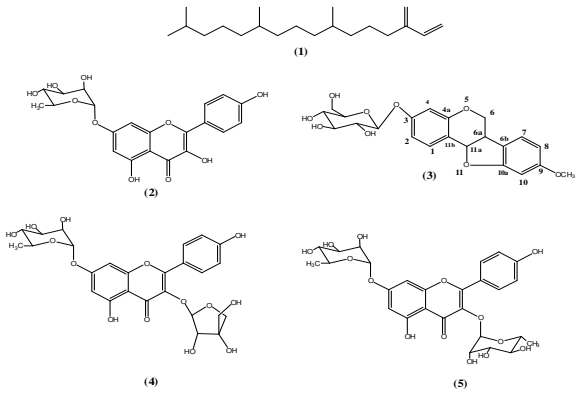

Fig. 1: Structures of isolated compounds (1-5)

Neophytadiene (7,11,15-trimethyl-3-methylidenehexadec-1-ene, 1) greyish white powder was identified as the major compound in the most potent cytotoxic sub-fraction PET-5 at 82.23 % using GCMS. It showed a molecular ion at m/z 278 (M^+) calc. for $C_{20}H_{38}$ and other fragments at 263 (M-CH_3)$^+$93, 179, 151, 137. 123,109, 95, 82, 68 (100) and 55 with Rt 32.195 min. The compound was identified using database of National Institute of Science and Technology version 17 (NIST17) and its mass and fragmentation pattern were compared with literature data (36). (Fig. 2,3)

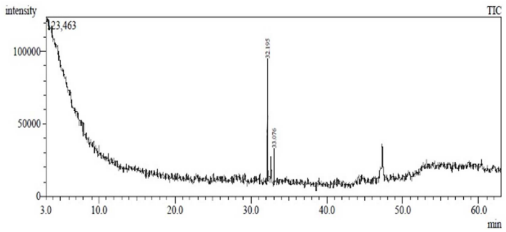

Fig. 2: GC chromatogram of compound (1)

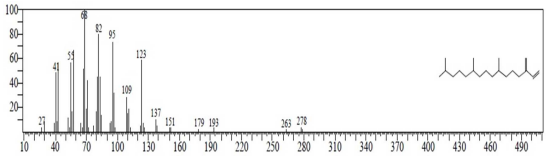

Fig. 3: EI-MS of compound (1)

Kaempferol-7-O-α-L-rhamnoside (2) yellowish amorphous powder, ^{1}H-NMR (DMSO-d_6, 400 MHz) δ 8.10 (1H d, 8.8 Hz, H-2`,6`), 6.94 (1H, d, 9.2 Hz, H-3`,5`) 6.84 (1H, d, 2 Hz, H-8), 6.43 (1H, d, 2 Hz, H-6), 5.55 (1H, d, 1.2 Hz, H-1``), 3.85 (1H, br s, H-2``), 3.62 (1H, m, H-3``), 3.45 (1H, m, H-5``), 3.3 (1H, m, H-4``) and 1.14 (3H, d, 6.0 Hz, H-6``), ^{13}C/APT NMR (DMSO- d_6, 100 MHz) δ 176.55 (CO, C-4), 161.89 (C, C-7), 160.85 (C, C-5), 159.85 (COH, C-4`), 156.21 (C, C-9), 147.97 (C, C-2), 136.51 (COH, C-3), 130.14 (CH, C-2`,6`), 122 (C, C1`), 115.94 (CH, C-3`,5`), 105.16 (C, C-10), 99.31 (CH, C-1``), 98.86 (CH ,C-6), 94.83 (CH, C-8), 72.07 (CH, C-4``), 70.72 (CH, C-3``), 70.55 (CH, C-2``), 70.32 (CH, C-5) and 18.40 (CH3, C6). ESI-MS showed 433 m/z (M+ H)$^+$calculated for $C_{21}H_{20}O_{10}$ and 287 (M- Rhamnose + H)$^+$ (Fig. 4-6) (37, 38).

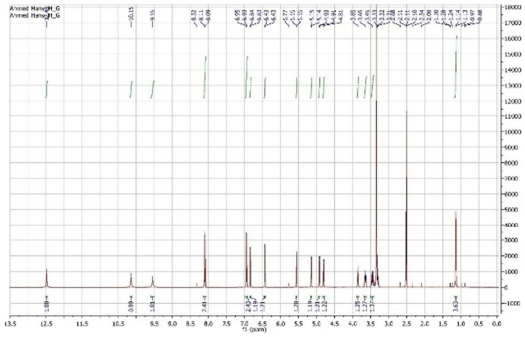

Fig. 4: ^{1}H NMR Spectrum of compound (2), (400 MHz, DMSO-d_6)

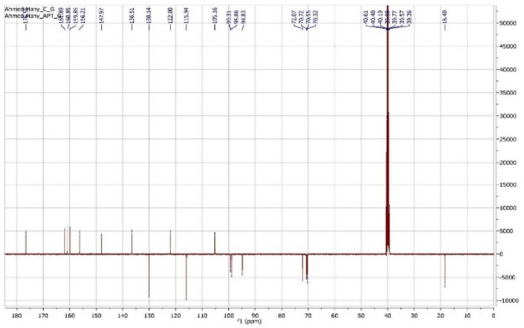

Fig. 5: ^{13}C/APT NMR Spectrum of compound (2), (100 MHz, DMSO-d_6)

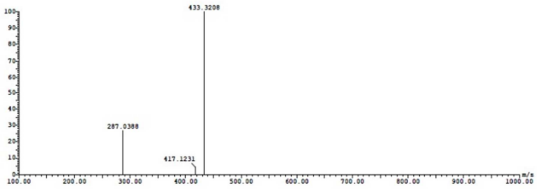

Fig. 6: ESI-MS of compound (2)

Medicarpin-3-O-*β*-D-glucopyranoside (3) Colorless crystals, ^{1}H-NMR (DMSO- d_6 , 400 MHz) δ 7.39 (1H, d, 8.4 Hz, H-1), 7.26 (1H, d, 8.4 Hz, H-7), 6.72 (1H, dd, 8.4, 2.4 Hz, H-2), 6.56 (1H, d, 2.4 Hz, H-4), 6.45 (1H, dd, 8 , 2 Hz, H-8), 6.43 (1H, d, 2 Hz, H-10), 5.61 (1H, d, 6.4 Hz, 1`), 5.30 (1H, d, 4.8

Hz, 11a), 4.15 (1H, m, H-6eq), 3.70 (1H, OCH3), 3.40 (1H, m, H-6a), 3.45 (1H,m, H-6ax) and 3.08-3.52 (m, H-2`-6`). ^{13}C/APT NMR (DMSO- d_6, 100 MHz) δ 161.01 (COCH3, C-9), 160.70 (C, C-10a), 159 (CO, C-3), 156.68 (CO, C-4a), 132.06 (CH, C-1), 125.65 (CH, C-7), 119.80 (C, C-6b), 114.65 (C-11b), 110.89 (CH, C-2), 106.59 (CH, C-10), 104.60 (CH, C-4), 100.80 (CO2H, C-1`), 96.82 (CH, C-8), 78.16 (CHO, C-11a), 77.52 (CHOH, C-3`), 76.98 (CH, C-5`), 73.64 (CHOH, C-2`), 70.16 (CHOH, C-4`), 66.40 (CH2O, C-6), 61.15 (CH2OH, C-6`), 55.76 (CH_3O) and 38.54 (CH, C-6a). ESI-MS 431 m/z $[M-H]^-$ (calc. for $C_{22}H_{24}O_9$). (Fig. 7-9)(39).

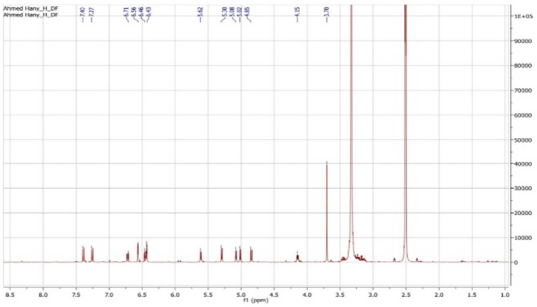

Fig. 7: ^{1}H NMR Spectrum of compound (3), (400 MHz, DMSO-d_6)

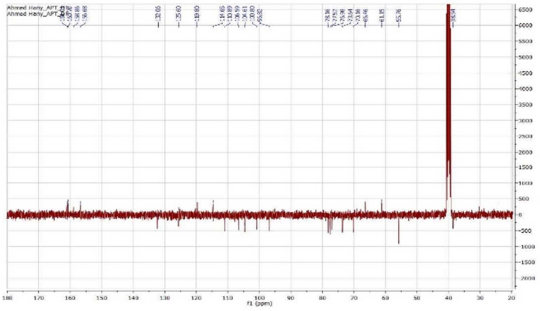

Fig. 8: ^{13}C/APT NMR Spectrum of compound (3), (100 MHz, DMSO-d_6)

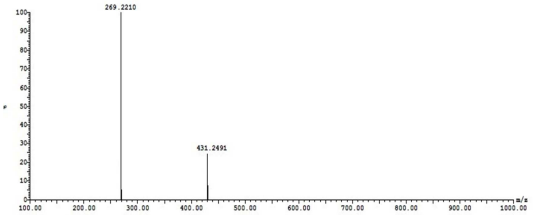

Fig. 9: ESI-MS of compound (3)

Kaempferol-3-O-β-D-apiofuranosyl-7-O-α-L-rhamnoside (4) yellowish amorphous powder, ^{1}H-NMR (DMSO- d_6, 400 MHz) δ 7.98 (1H, d, 8.8 Hz, H-2`, 6`), 6.92 (1H, d 8.8 Hz, H-3`, 5`), 6.83 (1H, d, 2 Hz, H-8), 6.46 (1H, d, 2 Hz, H-6), 5.74 (1H, d, 2 Hz, H-1``), 5.56 (1H, br s, H-1```), 4.2 (1H, br s, H-2``), 3.85 (1H, br s, H-2```), 3.62(1H, m, H-3```), 3.61 (1H, d, 9.6 Hz, H-4``eq), 3.50 (1H, d, 9.6 Hz, H-4``ax), 3.3-3.4 (3H, H-5``, H-4```, H-5```) and 1.13(3H, d, 6 Hz, CH_3). ^{13}C/APT NMR (DMSO- d_6, 100 MHz) δ 178.31 (CO, C-4), 162.10 (CO, C-7), 161.36 (COH, C-4`), 160.75 (COH, C-5), 157.82 (C, C-2), 156.46 (C, C-9),134.24 (CO, C3), 131.28 (CH, C-2`, 6`), 120.96 (C, C-1`), 116.03 (CH, C-3`, 5`), 109.73 (CO2H, C-1``), 106.14 (C, C-10), 99.85 (CH, C-6), 98.83 (CO2H, C-1```), 95.06 (CH, C-8), 79.89 (COH, C-3``), 77.65 (CHOH, C-2``), 75.66 (CH2, C-4``), 72.06 (CHOH, C-4```), 70.72(CHOH, C-3```), 70.55 (CHOH, C-2```), 70.28 (CH, C-5```), 63.24 (CH2OH, C-5``) and 18.37 (CH3, C-6```). ESI-MS 565.275 m/z $[M+H]^+$ (calc. for $C_{26}H_{28}O_{14}$) 433.122 m/z refers to $[M\text{-apiose}]^+$ 287.025 m/z correspond to $[M\text{- apiose - rhamnose}]^+$ (Fig. 10-12)(40, 41).

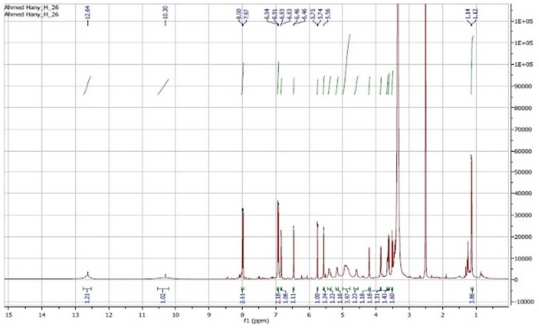

Fig. 10: ^{1}H NMR Spectrum of compound (4), (400 MHz,

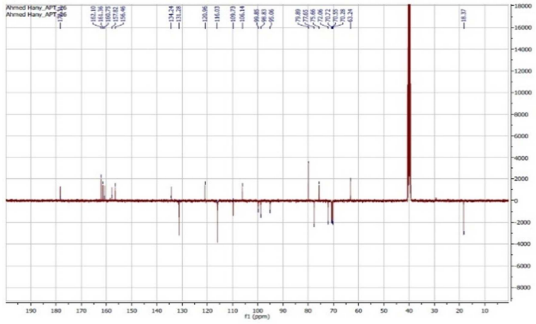

DMSO-d_6)

Fig. 11: ^{13}C/APT NMR Spectrum of compound (4), (100 MHz, DMSO-d6)

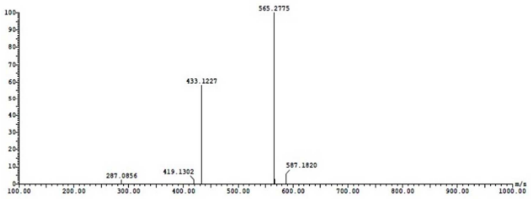

Fig. 12: ESI-MS of compound (4)

Kaempferitrin (Kaempferol-3,7-di-O-α-L-rhamnoside, 5) yellowish amorphous powder, ^{1}H-NMR (DMSO-d6, 400 MHz) δ 7.80 (1H, d, 8.8 Hz, H-2`, 6`), 6.93(1H, d, 8.8 Hz H-3`, 5`), 6.80 (1H, d, 2 Hz, H-8), 6.47 (1H, d, 2 Hz, H-6) , 5.56(1H, d, 1.2 Hz, H-1```), 5.31(1H, d, 1.6 Hz, H-1``), 3.99(1H, s, H-2``), 3.85 (1H, s, H-2```), 3.64 (1H, m, H-3``), 3.48 (1H, m, H-3```), 3.44 (1H, m, H-5```), 3.3 (1H, m, H-4```), 3.15 (1H, m, H-5``), 3.13(1H, m, H-4``), 1.14(3H, d, CH3) and 0.82 (3H, d, CH3). ^{13}C NMR (DMSO-d6, 100 MHz) δ 178.41 (CO, C-4) , 162.17 (CO, C-7), 161.4 (COH,C-5), 160.65 ` (COH, C4`), 158.27 (C, C-2), 156.57 (C, C-9), 135 (CO, C-3), 131.18 (CH, C-2`, 6`), 120.8 (C, C-1'), 115.9 (CH, C-3`, 5`), 106.26 (C, C-10), 102.34 (CH, C-1``), 99.94 (CH, C-6), 98.88 (CH, C-1```), 95.07 (CH, C-8), 72.05 (CHOH, C-4``), 71.56 (CHOH, C-4```), 70.78 (CHOH, C-3```), 70.69 (CHOH, C-2``), 70.56 (CHOH, C-2```), 70.54 (CH, C-5``), 70.28 (CH, C-5```), 71.15 (CHOH, C3``),18.83 (CH3, C-6```) and 17.90 (CH3, C6``). ESI-MS 579.295 m/z $[M+H]^{+}$ (calc. for $C_{27}H_{30}O_{14}$) The fragment at m/z 433.292 refers to $[M-\text{rhamnose}]^{+}$ and the fragment at m/z 287.025 correspond to $[M-2\ \text{rhamnose}]^{+}$. (Fig. 13-15)(42).

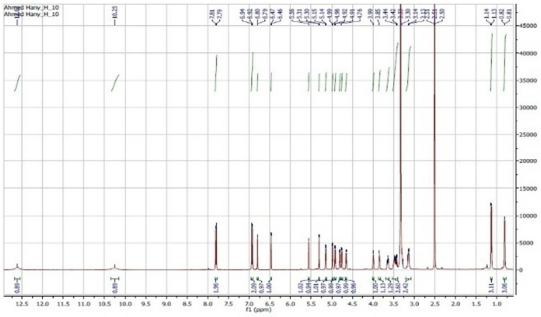

Fig. 13: ^{1}H NMR Spectrum of compound (5), (400 MHz, DMSO-d_6)

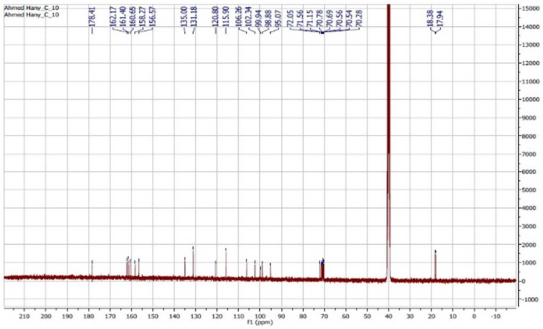

Fig. 14: ^{13}C NMR Spectrum of compound (5), (100 MHz, DMSO-d_6)

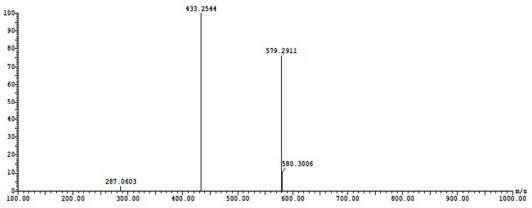

Fig. 15: ESI-MS of compound (5)

5. Molecular docking

Neophytadiene was screened against different targets that have main role in apoptotic activity. Neophytadiene showed high affinity mainly against Human A2a Receptor, Human LRH1 and hERG K+ channel which considered promising targets suits our compound. The binding interaction of neophytadiene exhibited binding energy -7.23 kcal/ mol against Human A2a Receptor. Neophytadiene formed twenty Pi-Alkyl and Pi-sigma interactions with Cys185, Val186, Trp246, Ile92, His250, Leu85, Leu249, Val84, Ile274 and Phe168 (Fig. 16).

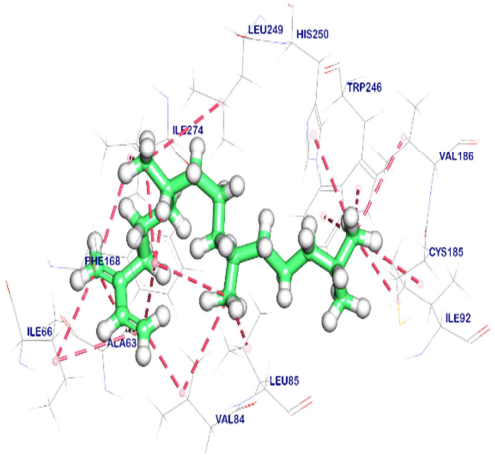

Fig. 16a

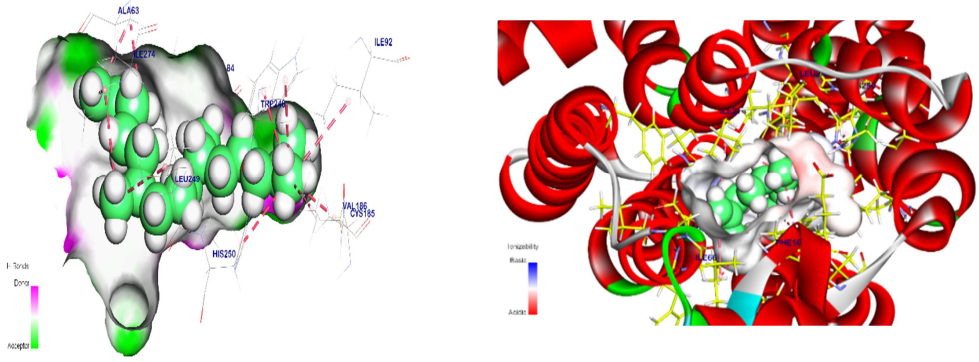

Fig. 16b **Fig. 16c**

Fig. 16: Neophytadiene docked in Human A2a Receptor, the pi interactions are represented in pink lines (Fig. 16a) with Mapping surface showing neophytadiene occupying the active pocket of Human A2a Receptor (Fig. 16b, 16c)

The binding mode of the co-crystalized ligand exhibited binding energy -8.46 kcal/ mol against Human LRH1 LBD. The crystal ligand formed eleven Pi-Alkyl, Pi-sulfur and Pi-Pi interactions with Met428, His390, Met345, Leu427, Ala513, Leu517, Ala349, Ile403 and Cys346. Additionally, interacted with Met345 by one hydrogen bond with a distance of 2.66 Å (Fig. 17).

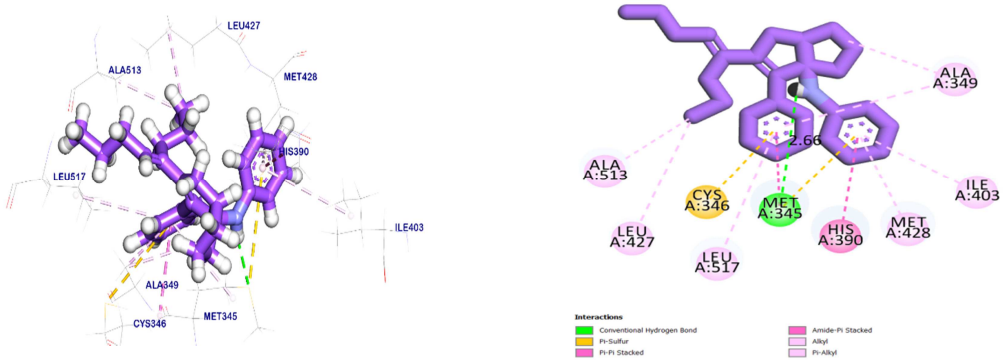

Fig. 17a **Fig. 17b**

Fig. 17: The co-crystalized ligand re-docked in Human LRH1 LBD, the pi interactions are represented in purple lines and the hydrogen bonds are represented in green lines (Fig. 17a) with Mapping surface showing Neophytadiene occupying the active pocket of Human LRH1 LBD (Fig. 17b)

The binding mode of Neophytadiene exhibited binding energy -9.01 kcal/ mol against Human LRH1 LBD. Neophytadiene formed thirteen Pi-Alkyl interactions with Met428, Ala431, His390, Met345, Leu405, Leu427, Ala513, Leu424, Ala349, Met348 and Val406 (Fig. 18).

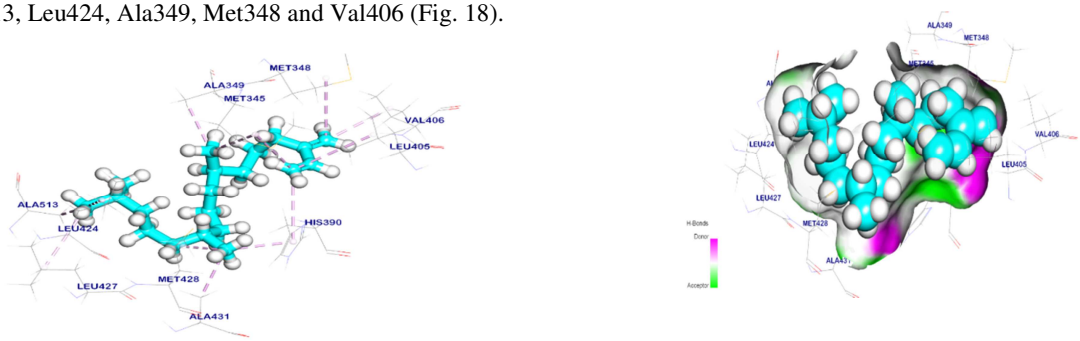

Fig.18a **Fig. 18b**

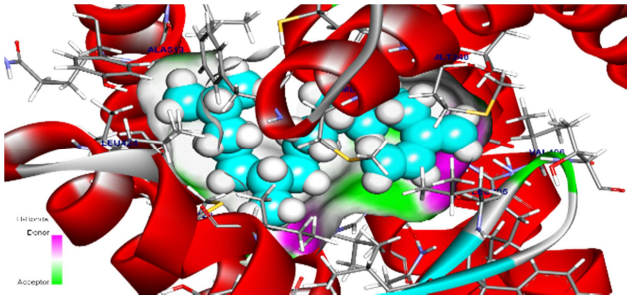

Fig. 18c

Fig. 18: Neophytadiene docked in Human LRH1 LBD, the pi interactions are represented in purple lines (Fig. 18a) with Mapping surface showing Neophytadiene occupying the active pocket of Human LRH1 LBD (Fig. 18b, 18c)

The binding mode of Neophytadiene exhibited binding energy -3.33 kcal/ mol against hERG K+ channel target site. Neophytadiene formed fifteen Pi-Alkyl interactions with Leu69, Pro98, Ile148, Trp143, Trp142, Phe33, Phe138, Val131, Leu132, Leu44, Phe48 and Ile123, (Fig. 19).

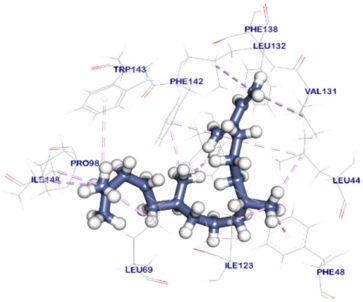

Fig. 19a

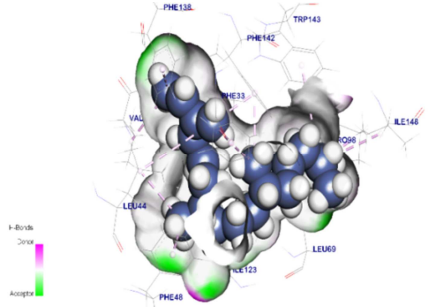

Fig. 19b

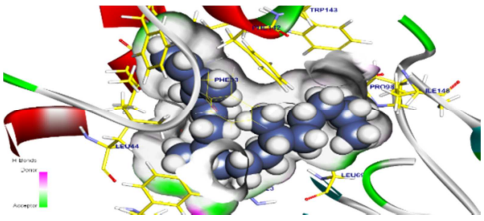

Fig. 19c

Fig. 19: Neophytadiene docked in hERG receptor the pi interactions are represented in faint purple lines (Fig. 19a) with Mapping surface showing Neophytadiene occupying the active pocket of hERG K+ channel (Fig. 19b, 19c)

Table (4)

Results of docked neophytadiene (DG, RMSD, interactions) kcal/mol against targeted sites of (Human A2a Receptor - Human LRH1 LBD – hERG K+ channel)

Targets screened	Tested compound	RMSD value (Å)	Docking score	Interactions	
			(kcal/mol)	Pi - interaction	H.B
HumanA2a Receptor	Neophytadiene	1.2	-7.23	20	-
Human LRH1 LBD	Neophytadiene	1.49	-9.01	13	-
	Co-crystalized ligand	1.01	-8.46	11	1
hERG K^+ channel	Neophytadiene	1.66	-3.33	15	-

H.B = Hydrogen bonds H.B = Hydrogen bonds

The mechanisms of neophytadiene with the three selected receptors are illustrated below (Fig. 20).

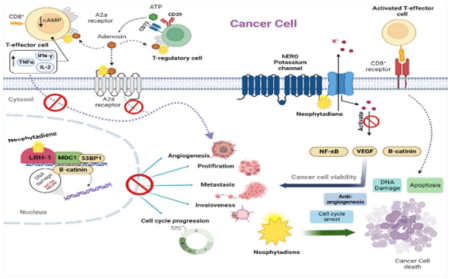

Fig. 20: Mechanism of Neophytadiene as apoptotic inducer on selected receptors

6. Conclusion

Diterpene neophytadiene (1) showed promising *in vitro* activity against A-549 and PC-3 which make it a suitable candidate for further *in vivo* studies for development of new anticancer drug. the *in silico* studies results in explanation of the possible mechanisms for neophytadiene activity on targeted receptors. Based on docking studies, neophytadiene showed high affinity towards Human LRH-1 and Human A2a Receptor. These receptors have multiple signalling pathways that have a critical role in cancer cell viability and invisibility. Neophytadiene may inhibit these pathways by interfering with adenosine target site in Human A2a Receptor, blocking Human LRH-1 and hERG K+ channel receptors led to cancer cell death, so it may act as promising apoptotic inducer.

7. Compliance with Ethical Standards

The study was carried out under ethical principles.

8. Conflict of interest

The authors declare that they have no conflict of interest.

9. References

1.El-Mernissi R, El Khatabi K, Khaldan A, El Mchichi L, Ajana MA, Lakhlifi T, et al. 3D-QSAR, ADMET, and Molecular Docking Studies for Designing New 1, 3, 5-Triazine Derivatives as Anticancer Agents. Egyptian Journal of Chemistry. 2022;65(13):9-18.

2.Mondal S, Bandyopadhyay S, K Ghosh M, Mukhopadhyay S, Roy S, Mandal C. Natural products: promising resources for cancer drug discovery. Anti-Cancer Agents in Medicinal Chemistry (Formerly Current Medicinal Chemistry-Anti-Cancer Agents). 2012;12(1):49-75.

3.Xia C, Dong X, Li H, Cao M, Sun D, He S, et al. Cancer statistics in China and United States, 2022: profiles, trends, and determinants. Chinese medical journal. 2022;135(05):584-90.

4.Jachak SM, Saklani A. Challenges and opportunities in drug discovery from plants. Current science. 2007:1251-7.

5.Benjamim JKF, da Costa KAD, Santos AS. Chemical, botanical and pharmacological aspects of the Leguminosae. Pharmacognosy Reviews. 2021;14(28).

6.El-Rafie HM, Mohammed RS, Abou Zeid AH, Sleem AA. Bioactivities and phytochemical studies of Acrocarpusfraxinifolius Bark Wight Arn. Egyptian Journal of Chemistry. 2020;63(1):203-14.

7.Usman M, Khan WR, Yousaf N, Akram S, Murtaza G, Kudus KA, et al. Exploring the Phytochemicals and Anti-Cancer Potential of the Members of Fabaceae Family: A Comprehensive Review. Molecules. 2022;27(12):3863.

8.Kim A, Ha J, Kim J, Cho Y, Ahn J, Cheon C, et al. Natural Products for Pancreatic Cancer Treatment: From Traditional Medicine to Modern Drug Discovery. Nutrients. 2021;13(11):3801.

9.Anugrahwati M, Purwaningsih T, Manggalarini J, Alnavis N, Wulandari D, Pranowo H. Extraction of ethanolic extract of red betel leaves and its cytotoxicity test on HeLa cells. Procedia engineering. 2016;148:1402-7.

10.dos Santos GS, Rangel KC, Teixeira TR, Gaspar LR, Abreu-Filho PG, Pereira LM, et al. GC-MS analysis, bioactivity-based molecular networking and antiparasitic potential of the Antarctic alga Desmarestia antarctica. Planta Medica International Open. 2020;7(03):e122-e32.

11.Hoseinzadeh A, Sadeghipour Y, Behbudi G. Investigation Preliminary antimicrobial and anticancer properties: on Topic Rubia tinctorum plant by using Polydimethylsiloxane (CAR/PDMS). Advances in Applied NanoBio-Technologies. 2020;1(1):10-9.

12.Li X, Zhang W, Qin Y, Xing X. Essential Oil from Hedyotischrysotricha: Chemical Composition, Cytotoxic, Antibacterial Properties and Synergistic Effects with Streptomycin. Records of Natural Products. 2022;16(4):376-81.

13. Bhardwaj M, Sali VK, Mani S, Vasanthi HR. Neophytadiene from Turbinariaornata suppresses LPS-induced inflammatory response in RAW 264.7 macrophages and Sprague Dawley rats. Inflammation. 2020;43(3):937-50.

14.Hashem MM, Salama MM, Mohammed FF, Tohamy AF, El Deeb KS. Metabolic profile and hepatoprotective effect of Aeschynomene elaphroxylon (Guill. & Perr.). PloS one. 2019;14(1):e0210576.

15.Dahab MA, Hegazy MM, Abbass HS. Hordatines as a potential inhibitor of COVID-19 main protease and rna polymerase: an in-silico approach. Natural products and bioprospecting. 2020;10(6):453-62.

16.Arcangeli A, Becchetti A. hERG Channels: From Antitargets to Novel Targets for Cancer TherapyhERG Channels and Cancer. Clinical Cancer Research. 2017;23(1):3-5.

17.Leone RD, Lo Y-C, Powell JD. A2aR antagonists: Next generation checkpoint blockade for cancer immunotherapy. Computational and structural biotechnology journal. 2015;13:265-72.

18.Stein S, Schoonjans K. Molecular basis for the regulation of the nuclear receptor LRH-1. Current opinion in cell biology. 2015;33:26-34.
19.Ohta A, Gorelik E, Prasad SJ, Ronchese F, Lukashev D, Wong MK, et al. A2A adenosine receptor protects tumors from antitumor T cells. Proceedings of the National Academy of Sciences. 2006;103(35):13132-7.
20.Bhat P, Leggatt G, Waterhouse N, Frazer IH. Interferon-γ derived from cytotoxic lymphocytes directly enhances their motility and cytotoxicity. Cell death & disease. 2017;8(6):e2836-e.
21.Sitkovsky M, Lukashev D, Deaglio S, Dwyer K, Robson S, Ohta A. Adenosine A2A receptor antagonists: blockade of adenosinergic effects and T regulatory cells. British journal of pharmacology. 2008;153(S1):S457-S64.
22.Jehle J, Schweizer P, Katus H, Thomas D. Novel roles for hERG K+ channels in cell proliferation and apoptosis. Cell death & disease. 2011;2(8):e193-e.
23.Lastraioli E, Lottini T, Bencini L, Bernini M, Arcangeli A. hERG1 potassium channels: novel biomarkers in human solid cancers. BioMed Research International. 2015;2015.
24.Patil VM, Gaurav A, Garg P, Masand N. Non-cancer to anti-cancer: investigation of human ether-a-go-go-related gene potassium channel inhibitors as potential therapeutics. Journal of the Egyptian National Cancer Institute. 2021;33(1):1-16.
25.Bayrer JR, Mukkamala S, Sablin EP, Webb P, Fletterick RJ. Silencing LRH-1 in colon cancer cell lines impairs proliferation and alters gene expression programs. Proceedings of the National Academy of Sciences. 2015;112(8):2467-72.
26.Ortlund EA, Lee Y, Solomon IH, Hager JM, Safi R, Choi Y, et al. Modulation of human nuclear receptor LRH-1 activity by phospholipids and SHP. Nature structural & molecular biology. 2005;12(4):357-63.
27.Schoonjans K, Dubuquoy L, Mebis J, Fayard E, Wendling O, Haby C, et al. Liver receptor homolog 1 contributes to intestinal tumor formation through effects on cell cycle and inflammation. Proceedings of the National Academy of Sciences. 2005;102(6):2058-62.
28.Wang S, Zou Z, Luo X, Mi Y, Chang H, Xing D. LRH1 enhances cell resistance to chemotherapy by transcriptionally activating MDC1 expression and attenuating DNA damage in human breast cancer. Oncogene. 2018;37(24):3243-59.
29.Gomha SM, Riyadh SM, Mahmmoud EA. Synthesis and anticancer activities of thiazoles, 1, 3-thiazines, and thiazolidine using chitosan-grafted-poly (vinylpyridine) as basic catalyst. Heterocycles: an international journal for reviews and communications in heterocyclic chemistry. 2015;91(6):1227-43.
30.Mosmann T. Rapid colorimetric assay for cellular growth and survival: application to proliferation and cytotoxicity assays. Journal of immunological methods. 1983;65(1-2):55-63.
31.McDonald S, Prenzler PD, Antolovich M, Robards K. Phenolic content and antioxidant activity of olive extracts. Food chemistry. 2001;73(1):73-84.
32.Chang C-C, Yang M-H, Wen H-M, Chern J-C. Estimation of total flavonoid content in propolis by two complementary colometric methods. Journal of food and drug analysis. 2002;10(3):3.
33.Rodríguez AM, Rosell G, BujonsVilàs J, Gutiérrez-de-Terán H, Rodríguez D, Brea JM, et al. Synthesis, biological activity and molecular docking analysis of new A2A adenosine receptor agonists. 2010.
34.Metwaly AM, Elkaeed EB, Alsfouk BA, Saleh AM, Mostafa AE, Eissa IH. The Computational Preventive Potential of the Rare Flavonoid, Patuletin, Isolated from Tagetes patula, against SARS-CoV-2. Plants. 2022;11(14):1886.
35.Herrera-Calderon O, Saleh AM, Yepes-Perez AF, Aljarba NH, Alkahtani S, Batiha GE-S, et al. Computational Study of the Phytochemical Constituents from Uncaria tomentosa Stem Bark against SARS-CoV-2 Omicron Spike Protein. Journal of Chemistry. 2022;2022.
36.Santos SA, Trindade SS, Oliveira CS, Parreira P, Rosa D, Duarte MF, et al. Lipophilic fraction of cultivated Bifurcariabifurcata R. Ross: Detailed composition and in vitro prospection of current challenging bioactive properties. Marine Drugs. 2017;15(11):340.
37.Marzouk MM. A comparative review on phytochemical constituents and biological effects of Melilotus indicus (L.) All. and Melilotus messanensis (L.) All.,(Fabaceae): evidence for chemosystematic analysis. Egyptian Journal of Chemistry. 2021.
38.Ragab N, El Sawi S, Marzouk M, El Halawany A, Sleem A, Farghaly A, et al. Chemical characterization of Melilotus messanensis (L.) all.: Antioxidant, antidiabetic and antimutagenic effects in alloxan induced diabetic rats. Biocatalysis and Agricultural Biotechnology. 2021;33:101976.
39.Li W, Koike K, Asada Y, Hirotani M, Rui H, Yoshikawa T, et al. Flavonoids from Glycyrrhiza pallidiflora hairy root cultures. Phytochemistry. 2002;60(4):351-5.

40.Harrath AH, Jalouli M, Oueslati MH, Farah MA, Feriani A, Aldahmash W, et al. The flavonoid, kaempferol-3-O-apiofuranosyl-7-O-rhamnopyranosyl, as a potential therapeutic agent for breast cancer with a promoting effect on ovarian function. Phytotherapy Research. 2021;35(11):6170-80.
41.Oueslati MH, Tahar LB, Harrath AH. Catalytic, antioxidant and anticancer activities of gold nanoparticles synthesized by kaempferol glucoside from Lotus leguminosae. Arabian Journal of Chemistry. 2020;13(1):3112-22.
42.Sajeli Begum A, Sahai M, Fujimoto Y, Asai K, Schneider K, Nicholson G, et al. A new kaempferol diglycoside from Datura suaveolensHumb. &Bonpl. ex. Willd. Natural product research. 2006;20(13):1231-6.